Articles in PresS. Am J Physiol Lung Cell Mol Physiol (April 10, 2015). doi:10.1152/ajplung.00351.2014

Characterization of spontaneous airspace enlargement in mice lacking microfibrillar-associated protein 4

Anne Trommelholt Holm[1], Helle Wulf-Johansson[1], Svend Hvidsten[2], Patricia Troest Jorgensen[1], Anders Schlosser[1], Bartosz Pilecki[1], Maria Ormhøj[1], Jesper Bonnet Moeller[1], Claus Johannsen[2], Christina Baun[2], Thomas Andersen[2], Jan Philipp Schneider[3], Jan Hegermann[3], Matthias Ochs[3], Alexander A. Götz[4], Holger Schulz[5,6], Martin Hrabě de Angelis[7,8,9], Jørgen Vestbo[10], Uffe Holmskov[1], and Grith Lykke Sorensen[1]

[1]Institute of Molecular Medicine, Faculty of Health Sciences, University of Southern Denmark, Odense, Denmark.

[2]Department of Nuclear Medicine, Odense University Hospital, Odense, Denmark.

[3]Institute of Functional and Applied Anatomy, Hannover Medical School, Hannover, Germany; Biomedical Research in Endstage and Obstructive Lung Disease Hannover (BREATH), Member of the German Center for Lung Research (DZL), Hannover, Germany; REBIRTH Cluster of Excellence, Hannover, Germany.

[4]Institute of Neuropathology, University of Göttingen, Göttingen, Germany.

[5]Institute of Lung Biology and Disease, Helmholtz Zentrum München; German Research Center for Environmental Health, Neuherberg, Germany; Member of the German Center for Lung Research.

[6]Institute of Epidemiology I, Helmholtz Zentrum München; German Research Center for Environmental Health, Neuherberg, Germany.

[7]German Mouse Clinic, Institute of Experimental Genetics, Helmholtz Zentrum München, German Research Center for Environmental Health, Neuherberg, Germany.

[8]Chair of Experimental Genetics, Center of Life and Food Sciences Weihenstephan, Technische Universität München, Freising-Weihenstephan, Germany.

[9]German Center for Diabetes Research (DZD), Neuherberg, Germany.

[10]Department of Respiratory Medicine, Gentofte Hospital, Hellerup, Denmark.

Corresponding author: Grith Lykke Sorensen, Institute of Molecular Medicine, Faculty of Health Sciences, University of Southern Denmark, JB Winsloews Vej 25.3, 5000 Odense, Denmark. Tel.: +4565503932. E-mail: glsorensen@health.sdu.dk.

Running head: Airspace enlargement in mice lacking MFAP4

Abstract

Microfibrillar-associated protein 4 (MFAP4) is localized to elastic fibers in blood vessels and the interalveolar septa of the lungs and is further present in bronchoalveolar lavage. *Mfap4* has been previously suggested to be involved in elastogenesis in the lung. We tested this prediction and aimed to characterize the pulmonary function changes and emphysematous changes that occur in *Mfap4* deficient (*Mfap4*$^{-/-}$) mice.

Significant changes included increases in total lung capacity and compliance, which were evident in *Mfap4*$^{-/-}$ mice at 6 months and 8 months, but not at 3 months of age. Using *in vivo* breath-hold gated micro-computed tomography (micro-CT) in 8-month-old *Mfap4*$^{-/-}$ mice, we found that the mean density of the lung parenchyma was decreased, and the low-attenuation area (LAA) was significantly increased by 14 % compared to *Mfap4*$^{+/+}$ mice. Transmission electron microscopy (TEM) did not reveal differences in the organization of elastic fibers, and there was no difference in elastin content, but borderline significant increase in elastin mRNA expression in 3-month-old mice. Stereological analysis showed that alveolar surface density in relation to the lung parenchyma and total alveolar surface area inside of the lung were both significantly decreased in *Mfap4*$^{-/-}$ mice by 25 % and 15 %, respectively.

The data did not support an essential role of MFAP4 in pulmonary elastic fiber organization or content, but indicated increased turnover in young *Mfap4*$^{-/-}$ mice. However, *Mfap4*$^{-/-}$ mice developed a spontaneous loss of lung function, which was evident at 6 months of age, and moderate airspace enlargement, with emphysema-like changes.

Keywords: Airspace enlargement, gene deficiency, MFAP4

Introduction

MFAP4 is a 36-kDa glycoprotein composed of a short N-terminal region comprising one cysteine residue and an Arg-Gly-Asp (RGD) integrin-binding motif, followed by a C-terminal fibrinogen-related domain (FReD) (51). The MFAP4 protein is a disulfide-linked dimer that forms higher homo-oligomeric structures via non-covalent interactions (26, 38). FReDs are found in various human proteins involved in distinct functions, including innate immunity, tissue growth, and remodeling (43).

MFAP4 is considered to be the human homolog to a 36-kDa microfibril-associated glycoprotein (MAGP-36) originally found to be localized to the elastin-microfibril interface in the porcine aorta (23). MFAP4 was later detected in a variety of both elastic and non-elastic tissues in various species (4, 44-46). In humans, this protein is highly expressed at sites that are rich in elastic fibers, including pulmonary arteries and the interalveolar walls of the lungs (19, 38, 49). Furthermore, it is present as a soluble protein in bronchoalveolar lavage (BAL) (38) and in systemic circulation (19, 28, 36).

It has been hypothesized that MFAP4 plays a role in maintaining the integrity of the extracellular matrix (ECM) in organs of high tensile strength, such as the aorta (45), in elastogenesis and elastic fiber formation (15, 20, 46), and in skin photoprotection e.g. through interactions with fibrillin (17, 20). Moreover, *in silico* studies have recently predicted that *Mfap4*$^{-/-}$ mice might develop pulmonary emphysema (4) and circulating levels of MFAP4 are associated to the severity in chronic obstructive lung disease, indicative for a role in disease (19).

We have generated *Mfap4*$^{-/-}$ mice and shown that MFAP4 is an integrin ligand involved in vascular smooth muscle proliferation both *in vitro* and *in vivo*. The mice are apparently healthy and breed normally (Schlosser-A et al., 2014, submitted manuscript).

In the present study, we set out to test the hypothesis that ablation of MFAP4 would lead to disturbed integrity of pulmonary elastic tissue and result in the spontaneous development of airspace enlargement and emphysema. We thus aimed to characterize the pulmonary effects related to *Mfap4* deficiency and to identify whether the loss of MFAP4 is associated with altered lung function and the loss of alveolar tissue. We used lung function measurements, *in vivo* breath-hold gated micro-CT, TEM and stereological analysis to characterize the airspace enlargement and pulmonary emphysema-like changes that occur in *Mfap4*$^{-/-}$ mice.

Materials and Methods

Animals

Mfap4$^{-/-}$ mice were generated as described in Schlosser et al. (Schlosser-A et al., 2014, submitted manuscript). *Mfap4*$^{-/-}$ mice were crossbred with C57BL/6N mice for 10 or more generations before they were used for experiments. Initial lung function screens and lung function analyses were performed on 3- and 6-month-old *Mfap4*$^{-/-}$ and wild-type (*Mfap4*$^{+/+}$) littermates. The mice were maintained in individually ventilated cages (IVC) (Ventirack, Biozone, Margate, UK) with *ad libitum* water and standard chow (Altromin no. 1324, GmbH & Co. KG, Lage, Germany). The tests performed on the 3- and 6-month-old mice were approved by the responsible authority of the district government of Upper Bavaria, Germany.

Eight-month-old female *Mfap4*$^{-/-}$ and *Mfap4*$^{+/+}$ littermates were used for lung function measurements, micro-CT and TEM analysis. The mice were maintained with feed and water provided *ad libitum* as described above. These mouse experiments were performed under a license obtained from the National Animal Experiments Inspectorate of Denmark (ref. no. 2012-15-2934-00525).

Lung function analysis of 3- and 6-month-old mice

Spontaneous breathing pattern was performed essentially as described by Reinhard et al. (2002) (34) and according to Fuchs et al. (2011) (13) in unrestrained 3- and 6-month-old male and female *Mfap4*$^{-/-}$ and *Mfap4*$^{+/+}$ littermate mice by plethysmography using a Buxco® system (Buxco® Electronics; Sharon, CT, USA).

Lung function measurements were performed in anesthetized, intubated mice by using a computer-controlled piston-type servo ventilator as applied for the Jackson Phenome Project (34, 41), (http://phenome.jax.org/db/q?rtn=projects/projdet&reqprojid =16) and in the German Mouse Clinic (13). Briefly, the ventilator provides for positive pressure ventilation and for defined respiratory maneuvers for lung function testing. With the setup the following signals are continuously monitored: flow and volume signals, airway opening and esophageal pressure, and concentrations of respiratory and test gases (Helium and $C_{18}O$) by means of magnetic sector field mass spectrometry. Total lung capacity (TLC) was determined from measurements of inspiratory capacity (IC, volume slowly inspired over 10 seconds from a relaxed expiratory level to a tracheal pressure of +30 cm H_2O) and functional residual capacity (FRC), which was determined by helium

dilution technique (a rebreathing volume of 80 % inspiratory reserve capacity labeled with 1 % He in 21 % O_2, balance N_2, was applied at a rate of 50/min for 15 cycles). Expiratory reserve volume (ERV) was defined as the volume slowly expired over 10 seconds from FRC to a tracheal pressure of -10 cm H_2O. The quasi-static compliance of the lung (C_L) was determined from the linear portion of the transpulmonary pressure–volume curve obtained during a 6-second lasting exhalation from TLC to residual volume. Dynamic compliance of the lung (CL_{dyn}) was determined at a respiratory rate of 130 min^{-1} from the transpulmonary pressure points of flow reversal, with the tidal volume set to 50 % of IC.

Lung function measurements in 8-month-old mice

Lung function measurements were performed in 8-month-old female *Mfap4*$^{-/-}$ and *Mfap4*$^{+/+}$ littermate mice. The mice were anesthetized by intraperitoneal injection of 0.1 mg/g body weight ketamine (Ketaminol Vet, Ketaminol Vet, MSD Animal Health, Ballerup, Denmark) and 0.01 mg/g body weight xylazine (Rompun Vet, Bayer, www.Bayer.com) solutions diluted in saline (9 mg/mL sodium chloride, Fresenius Kabi). The mice were tracheostomized using a shortened 18-G catheter (Angiocath™, Becton Dickinson, Dandy, UT, USA), which was secured with a 5-0 suture (Vicryl, Ethicon, www.Ethicon.com). The mice were connected to a flexiVent system (flexiVent®, SCIREQ©, Montreal, Canada) and ventilated with a tidal volume of 10 mL/kg, a respiratory rate (frequency) of 150 breaths/minute and positive end-expiratory pressure (PEEP) of 3 cmH_2O essentially as described in de Langhe et al., 2012 (7). The flexiVent ventilator was used both for regular ventilation and for delivery of the oscillatory signal. The constant-phase model described by Hantos *et al*., 1992 (16) was used to partition respiratory impedance into components representing the mechanical properties of the airways and parenchyma, where H is a coefficient for tissue elastance. Data were rejected if the coherence values ”coefficients of determination (CODs)” were below 0.95. All measurements were obtained using flexiWare 7.1.1 software.

In vivo breath-hold gated micro-CT imaging

Eight-month-old female *Mfap4*$^{-/-}$ and *Mfap4*$^{+/+}$ littermate mice were anesthetized, tracheostomized, connected to a flexiVent system, and placed in a supine position in a micro-CAT II scanner (Siemens Inveon Standard, Siemens Pre-Clinical Solutions, Knoxville, TN, US). The deep inflation inspiration pressure hold (DIIPH) protocol was used for *in vivo* breath-hold gated imaging using an updated version of FlexiWare software (7.2.2) (flexiVent®, SCIREQ, Montréal, Québec, Canada).

During a 360-degree rotation, 720 projections were acquired with a source voltage of 80 kV and a beam current of 500 μA. The magnification was set to medium resolution, and the source-to-detector distance equaled 39.7 cm. A total of 720 micro-CT projections were acquired during the iso-pressure breath-holds at 12 cmH_2O and a 600 ms duration. Normal breathing was induced between breath-holds. A recruitment maneuver was performed (inflation of the lungs to 30 cmH_2O) to prevent atelectasis. The total acquisition time was approximately 60 minutes, although the actual exposure time was limited to 7 minutes. The absorbed radiation dose of the animals was estimated by Dose Calculator software (Siemens Pre-Clinical Solutions, Knoxville, TN, US) to be approximately 750 mGy per scan.

Reconstruction of the projection data was performed with a filtered back projection Feldkamp algorithm and scaled to Hounsfields units (HUs) using acquisition software IAW version 1.5 (Siemens Pre-Clinical Solutions, Knoxville, TN, US). The reconstructed images had isotropic voxels of 79 μm in size. After scanning, the lungs were removed and prepared for TEM, light microscopy, and stereology.

Micro-CT image analysis

Image analysis was performed using Siemens Inveon Research Workplace 4.1 software (Siemens Pre-Clinical Solutions, Knoxville, TN, US), and the protocol was modified from Ford et al. (2009) (11). The lung volumes, CT density, and sizes of the major airways were measured from the 3D micro-CT images using thresholds and a seeded region-growing algorithm. The region of interest (ROI) was found using a semiautomatic procedure beginning with a coarse manual delineation of the entire lung. The threshold value for extracting lungs from background tissue was set to -210 Hounsfield units (HUs), and all contiguous voxels inside of the ROI with values of below -210 HUs were selected. Similarly, a threshold for extracting the major airways from the lung tissue was found (-800 HU), and the voxels corresponding to the major airways were selected. The volumes of the mainstem left and right bronchi were determined by the seeding region-growing algorithm and subtracted from that of the total lung, resulting in a ROI containing only the lung parenchyma. The voxels from this ROI were exported and rebinned to construct a graphical representation of the frequency distribution of the CT numbers. As in Kawakami et al. (2008), thresholds were set in the range of -800 HUs to -600 HUs for the lung parenchyma LAA (21). By applying these thresholds, the percentage of LAA (LAA%) was calculated as the ratio of LAA to the CT-derived lung area.

Perfusion fixation process

The fixation of the lungs for TEM, light microscopy, and stereology was performed as described by Fehrenbach and Ochs (1998) (9) and according to the guidelines of the American Thoracic Society/European Respiratory Society: Standards for Quantitative Assessment of Lung Structure (18). Briefly, the lungs were fixed *in situ* after the abdomen (bilateral pneumothorax) was opened and the pulmonary artery and veins were clamped by the intratracheal instillation of fixative (1.5 % paraformaldehyde and 1.5 % glutaraldehyde in 0.15 M Hepes buffer, pH 7.35) at a constant pressure of 25 cmH_2O until the flow stopped (approximately 5 minutes). The trachea was ligated below the tube insertion site, and the lungs were carefully removed from the thorax, immersed into the fixative and stored at 4°C until further processing.

Sampling for stereology, TEM and light microscopy

Samples for microscopic analysis were obtained by systematic uniform random sampling (SURS) (18, 29). After estimation of the total lung volume, *V*(lung) using Scherle's method (18, 22, 29, 37), the lungs were kept in the fixative at 4°C until further processing. The lungs were following embedded in agar and cut into slabs of roughly equal thickness (2 mm) using a tissue slicer (40). The agar slabs of the right and left lungs were separated and arranged in sequence. Beginning with a random start, every second slab was assigned to either light or electron microscopy. After the removal of the surrounding agar, the samples were stored in fixative until further processing. After postfixation with osmium tetroxide (OsO4) and uranyl acetate and stepwise dehydration in acetone the samples were embedded in glycol methacrylate (Technovit 8100, Heraeus Kulzer, Wehrheim, Germany) (compare Schneider and Ochs (2014) (39)). The remaining slices were used for qualitative TEM analysis. Regions containing macroscopically visible airways were cut out and embedded as described below.

TEM

Post-fixation of the lungs was accomplished by incubating them in 1 % osmium tetraoxide for 2 hours at room temperature followed by an incubation in half-saturated uranyl acetate overnight at 4°C (both solutions in water). The next day, the tissues were dehydrated stepwise in acetone and embedded in EPON (Serva, Heidelberg, Germany). Fifty-nanometer ultrathin sections were post-stained with uranyl acetate and lead citrate as previously described (35). The sections were analyzed

using a transmission electron microscope (Morgagni, FEI, Hillsboro, Oregon, USA) at 80 kV. Images were obtained with a 2 K sidemounted Veleta camera binned to 1 K.

Stereology and light microscopy

Glycol methacrylate-embedded tissue blocks were randomly chosen. The first and fourth sections of a consecutive row of sections (section thickness: 1.5 µm) were mounted onto one glass slide and stained with orcein or toluidine blue. The toluidine blue-stained sections were used for light microscopy.

The orcein-stained sections were scanned, and stereological analysis was performed using newCAST software (Visiopharm, Hoersholm, Denmark). The volume density of the parenchyma within the lung, V_V(par/lung), was estimated by point counting, and the alveolar surface density related to the lung parenchyma, S_V(alv/par), was estimated by intersection counting. Vv(par/lung) was multiplied by the total lung volume, V(lung), to obtain the absolute value per lung; the total volume of the parenchyma per lung, V(par, lung). S_V(alv/par) was multiplied by V_V(par/lung) and V(lung) to obtain the total alveolar surface area inside of the lung S(alv, lung)(29-31).

BAL

After euthanasia, lungs from 3- and 8-month-old mice were lavaged *in situ* with four sequential aliquots of 0.5 mL sterile PBS (DPBS, Gibco®, Invitrogen). BAL was recovered after 30 seconds by gentle aspiration. The recovered BAL aliquots were pooled for each individual mouse. The BAL samples were centrifuged at 4°C for 10 minutes, and cell-free supernatants (BAL fluid (BALF)) were stored at -80°C until further analysis.

Protein extraction from lung tissue

Half of the PBS-perfused and snap-frozen left lungs obtained from the 3-month-old and 8-month-old mice were transferred to 2-mL tubes (Nalgene™ Natural PPCO, Sigma-Aldrich, www.sigmaaldrich.com). Zirconium oxide beads (2.8 mm, Bertin Technologies, www.bertin-technologies.com/) and 300 µL RIPA buffer with protease inhibitors (cOmplete Tablets, Roche Life Science, www.lifescience.roche.com) were added, and the tissue was homogenized using a Precellys®24 homogenizer (www.precellys.com) according to the manufacturer's recommendations. Afterwards, the samples were incubated on ice for 10 minutes and then centrifuged for 10 minutes at 10,000 g and 4°C. The supernatants were transferred to fresh

Eppendorf tubes and stored at -80°C for further analysis. To normalize the protein concentrations prior to further analysis, the total protein concentrations were determined using the DC™ protein assay (Bio-Rad Laboratories, Inc., www.bio-rad.com) according to the manufacturer's recommendations.

RNA purification from lung tissue

PBS-perfused and snap-frozen lungs obtained from the 3-month-old and 8-month-old mice were placed into 2-mL tubes (Nalgene™ Natural PPCO, Sigma-Aldrich, www.sigmaaldrich.com) containing 1000 µL Trizol reagent (Invitrogen™, Life Technologies, www.lifetechnologies.com) and zirconium oxide beads (2.8 mm, Bertin Technologies, www.bertin-technologies.com), homogenized using a Precellys®24 homogenizer (www.precellys.com) according to the manufacturer's recommendations, and transferred to 1.5 mL RNase-free Eppendorf tubes. Afterwards, total RNA was purified according to the manufacturer's recommendations. RNA extractions were quantified with a NanoDrop spectrophotometer (www.nanodrop.com) by measuring optical density at 260 nm.

Quantitative real-time PCR (qPCR)

cDNA synthesis was performed using 1.5-2 µg of purified RNA with a QuantiTect Reverse Transcription Kit (Qiagen, www.qiagen.com) or M-MLV reverse transcriptase (Sigma Aldrich, www.sigmaaldrich.com) according to the manufacturer's recommendations. TaqMan Universal Master Mix II (4440040, Applied Biosystems, www.lifetechnologies.com) and TaqMan Gene Expression Assays (www.lifetechnologies.com) were used with the following TaqMan probes: *Mfap4* (Mm00840681), *Eln* (Mm00514670), *Tbp* (Mm00446971), and *Gapdh* (Mm99999915). Reactions were performed in triplicate with a StepOnePlus Real-Time PCR system (www.lifetechnologies.com). Relative mRNA levels were calculated using the $2^{\Delta\Delta C_T}$ method with qBase+ (Biogazelle, Zwijnaarde, Belgium). *Tbp* and *Gapdh* were both used as endogenous controls.

Elastin levels in lung tissue

The elastin content in lung tissue from 3- and 8-month-old mice was solubilized using the hot oxalic acid digestion method and quantified using the Fastin Elastin Assay kit (Biocolor, Carrickfergus, UK) according to manufacture's instructions. Obtained results were normalized to starting lung tissue wet weight.

MFAP4 levels in bronchoalveolar fluid and lung tissue

The measurements of MFAP4 levels in the BALF and total protein purified from the left lung were performed using the AlphaLISA technique as described by Wulf-Johansson et al. (2013) (49). Monoclonal antibodies (anti-MFAP4, HG-HYB 7-14, anti-MFAP4, and HG-HYB 7-18) were raised against human recombinant MFAP4 (36) but cross-reacted with the murine MFAP4 homolog due to high sequence similarity. rMFAP4 concentrations are shown as U/mL, where 1 U/mL = 38 ng/mL in human serum.

Statistical analysis

Data were normally distributed and ANOVA and two-tailed unpaired *t*-tests were used to compare the corresponding values between groups. The results are presented as the means ± SEM. A nominal P-value < 0.05 was considered statistically significant. The graphical representations were produced using Prism v6.0c (GraphPad Software Inc. San Diego, CA, USA).

Results

Lung function measurements

Lung function measurements were performed for both the male (data not shown) and female mice, but statistical significance was only found in the female mice. Both TLC and ERV were significantly increased from 3 to 6 months of age and ERV was significantly increased in the 6-month-old *Mfap4*$^{-/-}$ mice compared to the *Mfap4*$^{+/+}$ littermates (**Figure 1A-B**). The functional residual capacity, vital capacity, volume of dead space, alveolar capillary gas exchange and resistance were not altered significantly (data not shown). The static and dynamic lung compliances were significantly increased in the 6-month-old *Mfap4*$^{-/-}$ mice compared to the *Mfap4*$^{+/+}$ littermates (**Figure 1C-D**).

Lung function measurements in the 8-month-old female *Mfap4*$^{-/-}$ mice supported the initial findings for the 6-month-old *Mfap4*$^{-/-}$ mice. The 8-month-old *Mfap4*$^{-/-}$ mice showed significantly increased TLC, dynamic compliance, static compliance and hysteresis compared to the *Mfap4*$^{+/+}$ littermates (**Figure 2A-D**). Moreover, tissue elastance (H) was significantly decreased in the *Mfap4*$^{-/-}$ mice (**Figure 2E**).

Evaluation of lung parenchymal density by micro-CT

Figure 3 shows slices through the lungs of an *Mfap4*$^{+/+}$ mouse and an *Mfap4*$^{-/-}$ mouse obtained by micro-CT scans. The lungs of the *Mfap4*$^{-/-}$ mouse appeared darker, indicating a higher air content. The graphical representation of the frequency distribution of the CT-numbers revealed that low CT numbers were most frequent in the *Mfap4*$^{-/-}$ mice, as demonstrated by the leftward shift in the lung density histogram (**Figure 4A**). Further analysis revealed that the lung volume was insignificantly increased when assessed by micro-CT and that the mean density of the lung parenchyma in the *Mfap4*$^{-/-}$ mice was significantly decreased compared to the *Mfap4*$^{+/+}$ mice (**Figure 4B-E**). For quantitative assessments, areas from -800 HUs to -600 HUs were used for the determination of low-density areas (low-attenuation areas, LAAs) in the lung parenchyma. The volume of the LAA was significantly increased by 55 % in the *Mfap4*$^{-/-}$ mice relative to the *Mfap4*$^{+/+}$ mice (0.45 ± 0.05 mL and 0.29 ± 0.03 mL, respectively) (**Figure 4F**). In addition, a significant decrease in the mean density of the LAA was observed in the *Mfap4*$^{-/-}$ mice compared with the *Mfap4*$^{+/+}$ mice (**Figure 4G**), and the LAA% was significantly increased by 14.2 % (51.0 ± 3.5 % and 36.8 ± 2.9 %, respectively) (**Figure 4H**).

Light microscopy and TEM of the lungs

A total of 8 *Mfap4*$^{+/+}$ and 7 *Mfap4*$^{-/-}$ 8-month-old female mice were analyzed by light microscopy and TEM. The distal airspaces in the lungs of the *Mfap4*$^{+/+}$ mice were inflated, indicating appropriate fixation (**Figure 5A**). They were further enlarged in the *Mfap4*$^{-/-}$ mice compared with the *Mfap4*$^{+/+}$ mice (**Figure 5B**). At the electron microscopic level, the structures of the ECM fibers in different blood vessels, ranging from muscularized arteries to capillaries in the alveolar septa, were highly heterogeneous. Regions with both very tight layers of elastic fibers and rather low densities were found. However, no apparent differences were observed between the *Mfap4*$^{-/-}$ and *Mfap4*$^{+/+}$ mice (**Figure 5C** and **Figure 5D**).

Elastin expresssion in 3- and 8-month-old Mfap4$^{+/+}$*and Mfap4*$^{-/-}$ *mice*

Elastin protein levels in lung tissue homogenates were equal in *Mfap4*$^{-/-}$ and *Mfap4*$^{+/+}$ mice (**Figure 6A and B).** There was a borderline significant increase in *Mfap4* mRNA synthesis in 3-month-old mice, which was not observed in 8-month-old mice (**Figure 6C and D**).

Stereology

Total lung volume, *V*(lung), the volume density of the parenchyma in relation to the lung volume, V_v(par/lung), and the total volume of parenchyma per lung, *V*(par, lung) were not significantly different in *Mfap4*$^{-/-}$ mice relative to *Mfap4*$^{+/+}$ (**Figure 7B-D**). Yet, the density of the alveolar surface in relation to the lung parenchyma, *S*(alv, lung), and the total alveolar surface area inside of the lung, *S*(alv/lung), were significantly decreased in the *Mfap4*$^{-/-}$ mice compared to the *Mfap4*$^{+/+}$ mice by 25 % (543.3 ± 27.6 cm^{-1} versus 723.9 ± 22.2 cm^{-1}) and 15 % (384.4 ± 11.2 versus 454.8 ± 30.3), respectively (**Figure 7E-F**). The micro-CT assessed LAA% was significantly inversely correlated to the stereology assessed *S*(alv, lung) ($r^2 = 0.62$, P = 0.001) (**Figure 7G**).

MFAP4 levels in 3- and 8-month-old Mfap4$^{+/+}$*mice*

MFAP4 expression was quantified at protein (lung tissue and BALF) and mRNA (lung tissue) levels in 3- and 8-month-old *Mfap4*$^{+/+}$ mice (**Figure 8**). Only the MFAP4 lung protein level was significantly increased in the 8-month-old *Mfap4*$^{+/+}$ mice compared with the 3-month-old *Mfap4*$^{+/+}$ mice ($P < 0.01$), whereas the BALF MFAP4 and *Mfap4* expression levels were non-significantly increased. There was no detectable MFAP4 expression in *Mfap4*$^{-/-}$ mice (data not shown).

Discussion

In the present study, we investigated the lung morphologies of *Mfap4*$^{-/-}$ mice using lung function measurements, breath-hold gated micro-CT imaging, TEM and stereology. The data did not support an essential role of MFAP4 in pulmonary elastin homeostasis, yet supported a protective role of MFAP4 in the maintenance of airspace and alveolar surface in adult mice under physiological conditions.

Lung function testing of 3- and 6-month-old mice was performed at the German Mouse Clinic (www.mouseclinic.de). "Level 1" examinations are used for screening of several groups with divergent age and gender and consist of spontaneous breathing measurements during rest and activity in unrestrained mice by whole body plethysmography from Buxco, but only "Level 2" examinations for lung function screening (13) has been presented in the present work. For the consecutive investigations of the *Mfap4*$^{-/-}$ pulmonary phenotype at 8 months of age the invasive flexiVent system (forced oscillation technique) was applied. The flexivent-based technique was necessary in order to perform breath-hold gating during micro-CT analysis in 8-month-old mice, because the tracheostomized mouse could be placed directly in the scanner. Both systems, the Level 2 "German Mouse Clinic System" and the flexiVent are well established systems and used for functional evaluation of lung disease models and for quantification of parenchymal disease via changes in e.g. total lung capacity and compliance of the respiratory system (47). A limitation of the study is that lung functions measurements obtained with the two different techniques are not directly comparable. Yet, the same direction of effects was seen with both techniques.

Initial observations using whole-body plethysmography revealed significant changes in the spontaneous breathing patterns of the *Mfap4*$^{-/-}$ female mice. The same tendencies were observed in male mice, but the differences did not reach statistical significance with the investigated male group sizes and suggested that the males were less susceptible to the loss of lung function. Significant differences in lung function between inbred male and female mice is previously documented (34) and some features are suggested regulated by female hormones (27, 48). The observations are further in accordance with previous clinical results indicating that the annual decline in lung density occurs the most rapidly in women (6). Only female mice were used for residual analyses. Significant increases in total lung capacity, compliance, and expiratory reserve volume were observed in the 6-month-old *Mfap4*$^{-/-}$ mice. The corresponding differences were of smaller magnitude and did not reach significance in 3-month-old mice. The findings suggest that the 6-month-old *Mfap4*$^{-/-}$ mice had to compensate for worsened mechanical properties and gas exchange

of their lungs. Following, we investigated lung mechanics via lung function measurements in the 8-month-old mice, which supported the initial observations and further showed that the *Mfap4*$^{-/-}$ mice had decreased tissue elasticity (decreased H) and significantly increased hysteresis that most likely reflects the more distensible alveoli.

The main advantage of micro-CT is that this method can be performed *in vivo*; thus, the original shapes and volumes of the lungs are preserved. To minimize ventilation errors and obtain the most reliable data, we chose to tracheostomize the mice instead of using endotracheal intubation during ventilation (8). The micro-CT images of the lungs of the 8-month-old *Mfap4*$^{-/-}$ mice appeared darker relative to the controls due to lower density of parenchymal tissue, but there were no signs of emphysematous bullae or clear emphysematous regions, suggesting a homogeneous distribution of airspace enlargement.

The normal human lung has a symmetrical distribution of HU values around a mean of approximately -800 HUs (5), whereas the mean density of the normal murine lung is considerably higher. In our study, the mean density of the normal lung (including the airways) was found to be -547.5 ± 5.7 HUs. The mean density of the lungs reported here are similar to those reported by Plathow et al. (2004) for C57BL/6J female mice of the same age (-561 HUs) without respiratory gating (32). Other studies have reported both higher and lower mean densities (2, 3, 12, 24, 33, 52). The varying values can be explained by the use of the iso-pressure breath-hold respiratory-gating technique for image acquisition, variations in the ages or strains of the animals, or differences in the scaling of images into CT values (10). The frequency distribution revealed that low CT values were the most pronounced in the *Mfap4*$^{-/-}$ mice. Areas of lower than -600 HUs, which were recognized as low-density areas (LAA%), were significantly increased as previously described in emphysematous lungs of murine models (12, 21, 24, 33). The low-density areas in the whole lungs of the wild-type mice were mainly restricted to the airways, whereas the corresponding areas in the *Mfap4*$^{-/-}$ mice were expanded to the lung parenchyma. Moreover, a significantly lower tissue elasticity and increased compliance were found in the 8-month-old *Mfap4*$^{-/-}$ mice. The 3D approach supported the initial observations of a lower tissue density and uniform airspace enlargement in the *Mfap4*$^{-/-}$ mice. Furthermore, the 3D images revealed that low-density areas were present in the center and at the base of the lung, as previously observed in several genetic models of emphysema that developed airspace enlargement in the adult mice (e.g., Smad3 (12), TIMP-3 (11), Pallid (50) and SAM (14)).

Airspace enlargement in aging *Mfap4*$^{-/-}$ mice may be caused by an inherent fragility of the alveolar walls, which would cause them to be prone to rupture by mechanical forces during

breathing (25, 42). TEM images of the lungs provided no evidence of changes in the ECM in the alveolar walls of the *Mfap4*$^{-/-}$ mice. Nevertheless, stereological analysis revealed decreases in the alveolar surface density, S_v(alv/par), and total alveolar surface of the lung, *S*(alv, lung), in the *Mfap4*$^{-/-}$ mice and demonstrated that the airspace enlargement was accompanied by emphysema-like changes. We observed a moderate, but significant, inverse correlation between micro-CT assessed LAA% and stereology assessed *S*(alv, lung), which showed that the two different approaches for assessing alveolar tissue density supported each other, and further suggests that the increased LAA% partly represents rupture related airspace enlargement.

MFAP4 has previously been proposed to mechanistically affect elastogenesis or maintenance of ECM fiber integrity (4, 45). Our observations did not fully support the original suggestions as we found identical elastin contents in *Mfap4*$^{+/+}$ and *Mfap4*$^{-/-}$ mice under physiological conditions. However, we found a tendency for transiently increased *Mfap4* mRNA expression, which indicates that synthesis as well as breakdown of elastin may be increased in young *Mfap4*$^{-/-}$ mice, possibly affecting pulmonary structure in later life.

We found significantly increased levels of MFAP4 in the lung parenchyma of the 8-month-old wild-type mice, which was accompanied by non-significant increases in BALF MFAP4 and *Mfap4 m*RNA. This observation suggests that MFAP4 is regulated to compensate for the normal airspace enlargement that occurs in aging mice. The data further suggest that posttranslational mechanisms may be involved in the regulation of tissue levels of MFAP4 in line with previous observations (1).

In summary, the data indicate that MFAP4 has no non-redundant role in the regulation of elastic fiber content or organization. However, MFAP4 participates in maintaining the integrity of the alveolar septa, and the ablation of MFAP4 resulted in airspace enlargement, decreased densities of the lung parenchyma, alveolar surface, and impairment of lung function occurring in adult mice. We conclude that *Mfap4* deficiency accelerates the development of airspace enlargement accompanied by emphysema-like changes. Further studies are warranted to unravel the mechanistic functions of MFAP4 in pulmonary physiology.

Acknowledgements

We especially thank the medical laboratory technician Vicki Nielsen (Institute of Molecular Medicine, Faculty of Health Science, University of Southern Denmark, Odense, Denmark) for measuring the MFAP4 levels using the AlphaLISA technique and for conducting the qPCR.

Furthermore, we thank the radiologist Stevo Duvnjak, Department of Radiology, Odense University Hospital, Odense, Denmark, for help with the interpretation of the micro-CT images.

Grants

This work was supported by the Danish Strategic Research Council, Center of COPD research (www.cekol.dk), Th. Maigaards Benthine Lunds Fond af 1.6.1978, Familien Hede Nielsens Fond, Fonden til Lægevidenskabens Fremme, and the German Federal Ministry of Education and Research (Infrafrontier grant 01KX1012).

Disclosures

AS, UH and GLS have issued the following patent: MFAP4 binding antibodies blocking the interaction between MFAP4 and integrin receptors (P1183DK00). JV has not received any financial support in relation to the current manuscript. Outside of this work, he has received honoraria for advising and presenting from AstraZeneca, Boehringer-Ingelheim, Chiesi, GSK, and Novartis.

References

1. **Aoki K, Harashima A, Sano M, Yokoi T, Nakamura S, Kibata M, and Hirose T.** A thymus-specific noncoding RNA, Thy-ncR1, is a cytoplasmic riboregulator of MFAP4 mRNA in immature T-cell lines. *BMC molecular biology* 11: 99, 2010.
2. **Artaechevarria X, Blanco D, de Biurrun G, Ceresa M, Perez-Martin D, Bastarrika G, de Torres JP, Zulueta JJ, Montuenga LM, Ortiz-de-Solorzano C, and Munoz-Barrutia A.** Evaluation of micro-CT for emphysema assessment in mice: comparison with non-radiological techniques. *European radiology* 21: 954-962, 2011.
3. **Artaechevarria X, Blanco D, Perez-Martin D, de Biurrun G, Montuenga LM, de Torres JP, Zulueta JJ, Bastarrika G, Munoz-Barrutia A, and Ortiz-de-Solorzano C.** Longitudinal study of a mouse model of chronic pulmonary inflammation using breath hold gated micro-CT. *European radiology* 20: 2600-2608, 2010.
4. **Brandsma CA, van den Berge M, Postma DS, Jonker MR, Brouwer S, Pare PD, Sin DD, Bosse Y, Laviolette M, Karjalainen J, Fehrmann RS, Nickle DC, Hao K, Spanjer AI, Timens W, and Franke L.** A large lung gene expression study identifying fibulin-5 as a novel player in tissue repair in COPD. *Thorax* Jul 2. pii: thoraxjnl-2014-205091. doi: 10.1136/thoraxjnl-2014-205091, 2014.
5. **Coxson HO.** Computed tomography and monitoring of emphysema. *The European respiratory journal* 29: 1075-1077, 2007.
6. **Coxson HO, Dirksen A, Edwards LD, Yates JC, Agusti A, Bakke P, Calverley PM, Celli B, Crim C, Duvoix A, Fauerbach PN, Lomas DA, Macnee W, Mayer RJ, Miller BE, Muller NL, Rennard SI, Silverman EK, Tal-Singer R, Wouters EF, Vestbo J, and Evaluation of CLtIPSEI.** The presence and progression of emphysema in COPD as determined by CT scanning and biomarker expression: a prospective analysis from the ECLIPSE study. *The Lancet Respiratory medicine* 1: 129-136, 2013.
7. **De Langhe E, Vande Velde G, Hostens J, Himmelreich U, Nemery B, Luyten FP, Vanoirbeek J, and Lories RJ.** Quantification of lung fibrosis and emphysema in mice using automated micro-computed tomography. *PloS one* 7: e43123, 2012.
8. **De Vleeschauwer SI, Rinaldi M, De Vooght V, Vanoirbeek JA, Vanaudenaerde BM, Verbeken EK, Decramer M, Gayan-Ramirez GN, Verleden GM, and Janssens W.** Repeated invasive lung function measurements in intubated mice: an approach for longitudinal lung research. *Laboratory animals* 45: 81-89, 2011.

9. **Fehrenbach H and Ochs M.** Studying lung ultrastructure. In: *Methods in Pulmonary Research*, edited by Uhlig S and Taylor AE. Basel: Birkhäuser Verlag, 1998, p. 429-454.

10. **Ford NL, Martin EL, Lewis JF, Veldhuizen RA, Drangova M, and Holdsworth DW.** In vivo characterization of lung morphology and function in anesthetized free-breathing mice using micro-computed tomography. *J Appl Physiol (1985)* 102: 2046-2055, 2007.

11. **Ford NL, Martin EL, Lewis JF, Veldhuizen RA, Holdsworth DW, and Drangova M.** Quantifying lung morphology with respiratory-gated micro-CT in a murine model of emphysema. *Physics in medicine and biology* 54: 2121-2130, 2009.

12. **Froese AR, Ask K, Labiris R, Farncombe T, Warburton D, Inman MD, Gauldie J, and Kolb M.** Three-dimensional computed tomography imaging in an animal model of emphysema. *The European respiratory journal* 30: 1082-1089, 2007.

13. **Fuchs H, Gailus-Durner V, Adler T, Aguilar-Pimentel JA, Becker L, Calzada-Wack J, Da Silva-Buttkus P, Neff F, Gotz A, Hans W, Holter SM, Horsch M, Kastenmuller G, Kemter E, Lengger C, Maier H, Matloka M, Moller G, Naton B, Prehn C, Puk O, Racz I, Rathkolb B, Romisch-Margl W, Rozman J, Wang-Sattler R, Schrewe A, Stoger C, Tost M, Adamski J, Aigner B, Beckers J, Behrendt H, Busch DH, Esposito I, Graw J, Illig T, Ivandic B, Klingenspor M, Klopstock T, Kremmer E, Mempel M, Neschen S, Ollert M, Schulz H, Suhre K, Wolf E, Wurst W, Zimmer A, and Hrabe de Angelis M.** Mouse phenotyping. *Methods* 53: 120-135, 2011.

14. **Fukuchi Y.** The aging lung and chronic obstructive pulmonary disease: similarity and difference. *Proceedings of the American Thoracic Society* 6: 570-572, 2009.

15. **Furuichi H, Yamashita K, Okada M, Toyoshima T, Hata Y, Suzuki S, Itano T, Shishibori T, Tokumitsu H, and Kobayashi R.** Identification of tranilast-binding protein as 36-kDa microfibril-associated glycoprotein by drug affinity chromatography, and its localization in human skin. *Biochemical and biophysical research communications* 270: 1002-1008, 2000.

16. **Hantos Z, Daroczy B, Suki B, Nagy S, and Fredberg JJ.** Input impedance and peripheral inhomogeneity of dog lungs. *J Appl Physiol (1985)* 72: 168-178, 1992.

17. **Hirano E, Fujimoto N, Tajima S, Akiyama M, Ishibashi A, Kobayashi R, and Okamoto K.** Expression of 36-kDa microfibril-associated glycoprotein (MAGP-36) in human keratinocytes and its localization in skin. *Journal of dermatological science* 28: 60-67, 2002.

18. **Hsia CC, Hyde DM, Ochs M, and Weibel ER.** An official research policy statement of the American Thoracic Society/European Respiratory Society: standards for quantitative

assessment of lung structure. *American journal of respiratory and critical care medicine* 181: 394-418, 2010.

19. **Johansson SL, Roberts NB, Schlosser A, Andersen CB, Carlsen J, Wulf-Johansson H, Saekmose SG, Titlestad IL, Tornoe I, Miller B, Tal-Singer R, Holmskov U, Vestbo J, and Sorensen GL.** Microfibrillar-associated protein 4: A potential biomarker of chronic obstructive pulmonary disease. *Respiratory medicine* Sep;108(9):1336-44. doi: 10.1016/j.rmed.2014.06.003, 2014.

20. **Kasamatsu S, Hachiya A, Fujimura T, Sriwiriyanont P, Haketa K, Visscher MO, Kitzmiller WJ, Bello A, Kitahara T, Kobinger GP, and Takema Y.** Essential role of microfibrillar-associated protein 4 in human cutaneous homeostasis and in its photoprotection. *Scientific reports* 1: 164, 2011.

21. **Kawakami M, Matsuo Y, Yoshiura K, Nagase T, and Yamashita N.** Sequential and quantitative analysis of a murine model of elastase-induced emphysema. *Biological & pharmaceutical bulletin* 31: 1434-1438, 2008.

22. **Knudsen L, Ochs K, Boxler L, Tornoe I, Lykke-Sorensen G, Mackay RM, Clark HW, Holmskov U, Ochs M, and Madsen J.** Surfactant protein D (SP-D) deficiency is attenuated in humanised mice expressing the Met(11)Thr short nucleotide polymorphism of SP-D: implications for surfactant metabolism in the lung. *Journal of anatomy* 223: 581-592, 2013.

23. **Kobayashi R, Tashima Y, Masuda H, Shozawa T, Numata Y, Miyauchi K, and Hayakawa T.** Isolation and characterization of a new 36-kDa microfibril-associated glycoprotein from porcine aorta. *The Journal of biological chemistry* 264: 17437-17444, 1989.

24. **Kobayashi S, Fujinawa R, Ota F, Kobayashi S, Angata T, Ueno M, Maeno T, Kitazume S, Yoshida K, Ishii T, Gao C, Ohtsubo K, Yamaguchi Y, Betsuyaku T, Kida K, and Taniguchi N.** A single dose of lipopolysaccharide into mice with emphysema mimics human chronic obstructive pulmonary disease exacerbation as assessed by micro-computed tomography. *American journal of respiratory cell and molecular biology* 49: 971-977, 2013.

25. **Kononov S, Brewer K, Sakai H, Cavalcante FS, Sabayanagam CR, Ingenito EP, and Suki B.** Roles of mechanical forces and collagen failure in the development of elastase-induced emphysema. *American journal of respiratory and critical care medicine* 164: 1920-1926, 2001.

26. **Lausen M, Lynch N, Schlosser A, Tornoe I, Saekmose SG, Teisner B, Willis AC, Crouch E, Schwaeble W, and Holmskov U.** Microfibril-associated protein 4 is present in lung

washings and binds to the collagen region of lung surfactant protein D. *The Journal of biological chemistry* 274: 32234-32240, 1999.

27. **Massaro GD, Mortola JP, and Massaro D.** Estrogen modulates the dimensions of the lung's gas-exchange surface area and alveoli in female rats. *The American journal of physiology* 270: L110-114, 1996.

28. **Molleken C, Sitek B, Henkel C, Poschmann G, Sipos B, Wiese S, Warscheid B, Broelsch C, Reiser M, Friedman SL, Tornoe I, Schlosser A, Kloppel G, Schmiegel W, Meyer HE, Holmskov U, and Stuhler K.** Detection of novel biomarkers of liver cirrhosis by proteomic analysis. *Hepatology* 49: 1257-1266, 2009.

29. **Mühlfeld C, Knudsen L, and Ochs M.** Stereology and morphometry of lung tissue. *Methods Mol Biol* 931: 367-390, 2013.

30. **Mühlfeld C and Ochs M.** Quantitative microscopy of the lung: a problem-based approach. Part 2: stereological parameters and study designs in various diseases of the respiratory tract. *American journal of physiology Lung cellular and molecular physiology* 305: L205-221, 2013.

31. **Ochs M and Mühlfeld C.** Quantitative microscopy of the lung: a problem-based approach. Part 1: basic principles of lung stereology. *American journal of physiology Lung cellular and molecular physiology* 305: L15-22, 2013.

32. **Plathow C, Li M, Gong P, Zieher H, Kiessling F, Peschke P, Kauczor HU, Abdollahi A, and Huber PE.** Computed tomography monitoring of radiation-induced lung fibrosis in mice. *Investigative radiology* 39: 600-609, 2004.

33. **Postnov AA, Meurrens K, Weiler H, Van Dyck D, Xu H, Terpstra P, and De Clerck NM.** In vivo assessment of emphysema in mice by high resolution X-ray microtomography. *Journal of microscopy* 220: 70-75, 2005.

34. **Reinhard C, Eder G, Fuchs H, Ziesenis A, Heyder J, and Schulz H.** Inbred strain variation in lung function. *Mammalian genome : official journal of the International Mammalian Genome Society* 13: 429-437, 2002.

35. **Reynolds ES.** The use of lead citrate at high pH as an electron-opaque stain in electron microscopy. *The Journal of cell biology* 17: 208-212, 1963.

36. **Saekmose SG, Schlosser A, Holst R, Johansson SL, Wulf-Johansson H, Tornoe I, Vestbo J, Kyvik KO, Barington T, Holmskov U, and Sorensen GL.** Enzyme-linked

immunosorbent assay characterization of basal variation and heritability of systemic microfibrillar-associated protein 4. *PloS one* 8: e82383, 2013.

37. **Scherle W.** A simple method for volumetry of organs in quantitative stereology. *Mikroskopie* 26: 57-60, 1970.

38. **Schlosser A, Thomsen T, Shipley JM, Hein PW, Brasch F, Tornoe I, Nielsen O, Skjodt K, Palaniyar N, Steinhilber W, McCormack FX, and Holmskov U.** Microfibril-associated protein 4 binds to surfactant protein A (SP-A) and colocalizes with SP-A in the extracellular matrix of the lung. *Scandinavian journal of immunology* 64: 104-116, 2006.

39. **Schneider JP and Ochs M.** Alterations of mouse lung tissue dimensions during processing for morphometry: a comparison of methods. *American journal of physiology Lung cellular and molecular physiology* 306: L341-350, 2014.

40. **Schneider JP and Ochs M.** Stereology of the lung. *Methods in cell biology* 113: 257-294, 2013.

41. **Schulz H, Johner C, Eder G, Ziesenis A, Reitmeier P, Heyder J, and Balling R.** Respiratory mechanics in mice: strain and sex specific differences. *Acta physiologica Scandinavica* 174: 367-375, 2002.

42. **Suki B, Jesudason R, Sato S, Parameswaran H, Araujo AD, Majumdar A, Allen PG, and Bartolak-Suki E.** Mechanical failure, stress redistribution, elastase activity and binding site availability on elastin during the progression of emphysema. *Pulmonary pharmacology & therapeutics* 25: 268-275, 2012.

43. **Thomsen T, Schlosser A, Holmskov U, and Sorensen GL.** Ficolins and FIBCD1: soluble and membrane bound pattern recognition molecules with acetyl group selectivity. *Molecular immunology* 48: 369-381, 2011.

44. **Toyoshima T, Ishida T, Nishi N, Kobayashi R, Nakamura T, and Itano T.** Differential gene expression of 36-kDa microfibril-associated glycoprotein (MAGP-36/MFAP4) in rat organs. *Cell and tissue research* 332: 271-278, 2008.

45. **Toyoshima T, Nishi N, Kusama H, Kobayashi R, and Itano T.** 36-kDa microfibril-associated glycoprotein (MAGP-36) is an elastin-binding protein increased in chick aortae during development and growth. *Experimental cell research* 307: 224-230, 2005.

46. **Toyoshima T, Yamashita K, Furuichi H, Shishibori T, Itano T, and Kobayashi R.** Ultrastructural distribution of 36-kD microfibril-associated glycoprotein (MAGP-36) in human and

bovine tissues. *The journal of histochemistry and cytochemistry : official journal of the Histochemistry Society* 47: 1049-1056, 1999.

47. **Vanoirbeek JA, Rinaldi M, De Vooght V, Haenen S, Bobic S, Gayan-Ramirez G, Hoet PH, Verbeken E, Decramer M, Nemery B, and Janssens W.** Noninvasive and invasive pulmonary function in mouse models of obstructive and restrictive respiratory diseases. *American journal of respiratory cell and molecular biology* 42: 96-104, 2010.

48. **Wilborn WH.** Hormonal effects on oxygen consumption and histology of submandibular glands of mice (Mus musculus). *Comparative biochemistry and physiology* 27: 357-363, 1968.

49. **Wulf-Johansson H, Lock Johansson S, Schlosser A, Trommelholt Holm A, Rasmussen LM, Mickley H, Diederichsen AC, Munkholm H, Poulsen TS, Tornoe I, Nielsen V, Marcussen N, Vestbo J, Saekmose SG, Holmskov U, and Sorensen GL.** Localization of microfibrillar-associated protein 4 (MFAP4) in human tissues: clinical evaluation of serum MFAP4 and its association with various cardiovascular conditions. *PloS one* 8: e82243, 2013.

50. **Yoshida M, Sakiyama S, Kenzaki K, Toba H, Uyama K, Takehisa M, Kondo K, and Tangoku A.** Functional evaluation of pallid mice with genetic emphysema. *Laboratory investigation; a journal of technical methods and pathology* 89: 760-768, 2009.

51. **Zhao Z, Lee CC, Jiralerspong S, Juyal RC, Lu F, Baldini A, Greenberg F, Caskey CT, and Patel PI.** The gene for a human microfibril-associated glycoprotein is commonly deleted in Smith-Magenis syndrome patients. *Human molecular genetics* 4: 589-597, 1995.

52. **Zhou Z, Kozlowski J, and Schuster DP.** Physiologic, biochemical, and imaging characterization of acute lung injury in mice. *American journal of respiratory and critical care medicine* 172: 344-351, 2005.

Figure captions

Figure 1. Lung Function Analysis of 3- and 6-month-old Female *Mfap4*$^{+/+}$ and *Mfap4*$^{-/-}$ Mice. **A**) The total lung capacity at 30 cm H_2O pressure (TLC30), **B**) expiratory reserve volume (ERV), **C**) quasi-static lung compliance (C_L) and **D**) dynamic lung compliance ($C_L$dyn). Lung function measurements were performed in anesthetized, intubated female mice by using a computer-controlled piston-type servo ventilator (13, 34, 41). Bars present mean ± SEM (n = 10-12/group). *P < 0.05, **P < 0.01, ***P < 0.001, ****P < 0.0001.

Figure 2. Lung Function Analysis in 8-month-old Female *Mfap4*$^{+/+}$ and *Mfap4*$^{-/-}$ Mice. **A**) Total lung capacity (TLC), **B**) quasi-static compliance (Cst), **C**) respiratory system compliance (Crs), **D**) hysteresis (area of the PV loop, η), and **E**) tissue elasticity (H) were measured using a flexiVent system. Bars present mean ± SEM (n = 15-18/group). **P < 0.01, ***P < 0.001, and ****P < 0.0001.

Figure 3. Micro-CT Images and 2D Reconstructions of the Air Contents in the Lungs of 8-month-old Female *Mfap4*$^{+/+}$ and *Mfap4*$^{-/-}$ Mice. Micro-CT and 2D air content images are shown that illustrate the enlargement of airspaces in the lung parenchyma of 8-month-old female *Mfap4*$^{-/-}$ mice. The low-density regions were determined using a threshold of -800 HUs to -600 HUs. The red color is defined as low density (-800 HUs) and dark blue as high density (-600 HUs) (see spectrum scale). Axial (upper panel), coronal (mid panel), and sagittal (lower panel) micro-CT images are shown of lungs from *Mfap4*$^{+/+}$ (left panels) and *Mfap4*$^{-/-}$ (right panels) mice.

Figure 4. Micro-CT based quantification of Airspace-enlargement in 8-month-old Female *Mfap4*$^{+/+}$ and *Mfap4*$^{-/-}$ Mice. *Mfap4*$^{-/-}$ mice and *Mfap4*$^{+/+}$ wild-type littermates were scanned using breath-hold gated micro-CT. **A**) The voxel values inside of the lungs (-1000 HUs to -210 HUs without the mainstem bronchi) were used to create a frequency distribution histogram. The graph shows the frequency of CT numbers vs. the absolute HU values for the *Mfap4*$^{-/-}$ (light grey) and *Mfap4*$^{+/+}$ (dark grey) mice, respectively. The black area is the area-under-the-curve for *Mfap4*$^{-/-}$ mice. The low-attenuation area (LAA) was determined using the threshold of -800 Hounsfield units (HUs) to -600 HUs, and the LAA% was calculated using the ratio of LAA to the area of the micro-

692 CT-derived lung parenchyma. **B**) CT-derived total lung volume**, C**) CT-derived volume of the
693 parenchyma, **D**) Mean density of the total lung**, E**) Mean density of the lung parenchyma, **F**) LAA
694 volume, **G**) LAA (mean density), **H**) LAA%. HUs: Hounsfield units. Bars present mean ± SEM (n
695 = 6-7/group). $^{*}P < 0.05$ and $^{**}P < 0.01$.
696
697 **Figure 5. Representative Light Microscopic and Transmission Electron Microscopic Images**
698 **of the Lungs of 8-month-old Female *Mfap4*$^{+/+}$ and *Mfap4*$^{-/-}$ Mice.** Light microscopic images of
699 toluidine blue-stained lung sections obtained from **A)** *Mfap4*$^{+/+}$ and **B)** *Mfap4*$^{-/-}$ mice. Scale bar:
700 100 µm. **C)** and **D)** Representative electron micrographs of intra-acinar blood vessels at the bases of
701 the alveolar septa in *Mfap4*$^{+/+}$ **C)** and *Mfap4*$^{-/-}$ **D)** mice**.** Left: overview of a vessel. Right: higher
702 magnification of the boxed areas. Elastic fibers appear bright and are marked by arrowheads.
703
704
705 **Figure 6. Elastin Quantification in 3- and 8-month-old Female *Mfap4*$^{+/+}$ and *Mfap4*$^{-/-}$ Mice.**
706 Relative quantification of elastin content in lung tissue obtained from (A) 3-month-old and (B) 8-
707 month-old *Mfap4*$^{+/+}$ and *Mfap4*$^{-/-}$ mice and elastin (*Eln*) gene expression in (C) 3-month-old and
708 (D) 8-month-old *Mfap4*$^{+/+}$ and *Mfap4*$^{-/-}$ mice. Bars present mean ± SEM (n = 6-10/group).
709
710
711 **Figure 7. Lung Stereological Data from 8-month-old Female *Mfap4*$^{+/+}$ and *Mfap4*$^{-/-}$ Mice. A**)
712 The total lung volume, *V*(lung), was measured by Scherle's method and stereological analysis of **B**)
713 the total volume of parenchyma per lung, *V*(par, lung), **C**) the volume density of parenchyma in
714 relation to the lung volume, V_V(par/lung), **D**) the total alveolar surface area inside of the lung, *S*(alv,
715 lung), **E**) the alveolar surface density related to lung parenchyma, S_V(alv/par), and **F**) correlation
716 between S_V(alv/par) obtained by stereological analysis and LAA% obtained by micro-CT analysis.
717 Bars present mean ± SEM (n = 6-7/group). $^{*}P < 0.05$ and $^{***}P < 0.001$.
718
719
Figure 8. MFAP4 Levels in 3- and 8-month-old *Mfap4*$^{+/+}$ Mice. A) MFAP4 levels measured in bronchoalveolar lavage. **B)** MFAP4 levels measured in the total protein purified from lung tissue. **C)** *Mfap4* mRNA expression level in lung tissue. Bars present mean ± SEM (n = 7-14/group). **P < 0.01.
720
721

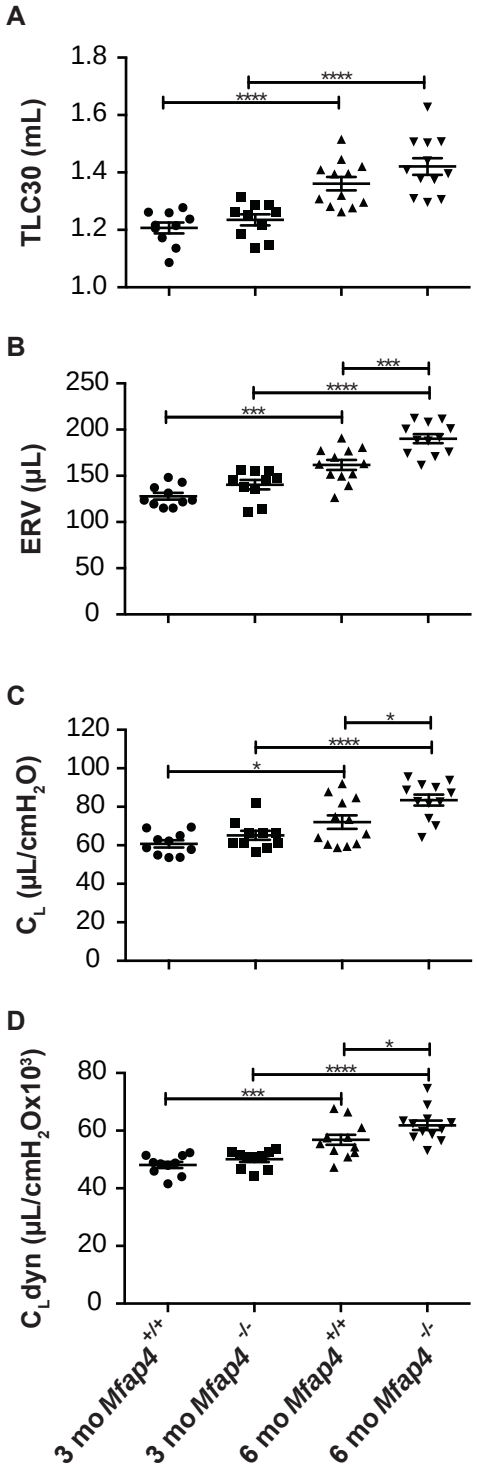
A
TLC30 (mL)
1.8
1.6
1.4
1.2
1.0
****
****
B
ERV (µL)
250
200
150
100
50
0
***
***
****
C
C_L (µL/cmH$_2$O)
120
100
80
60
40
20
0
*
*
****
D
$C_L$dyn (µL/cmH$_2$Ox10^3)
80
60
40
20
0
***
****
*
+/+
-/-
+/+
-/-
3 mo Mfap4
3 mo Mfap4
6 mo Mfap4
6 mo Mfap4

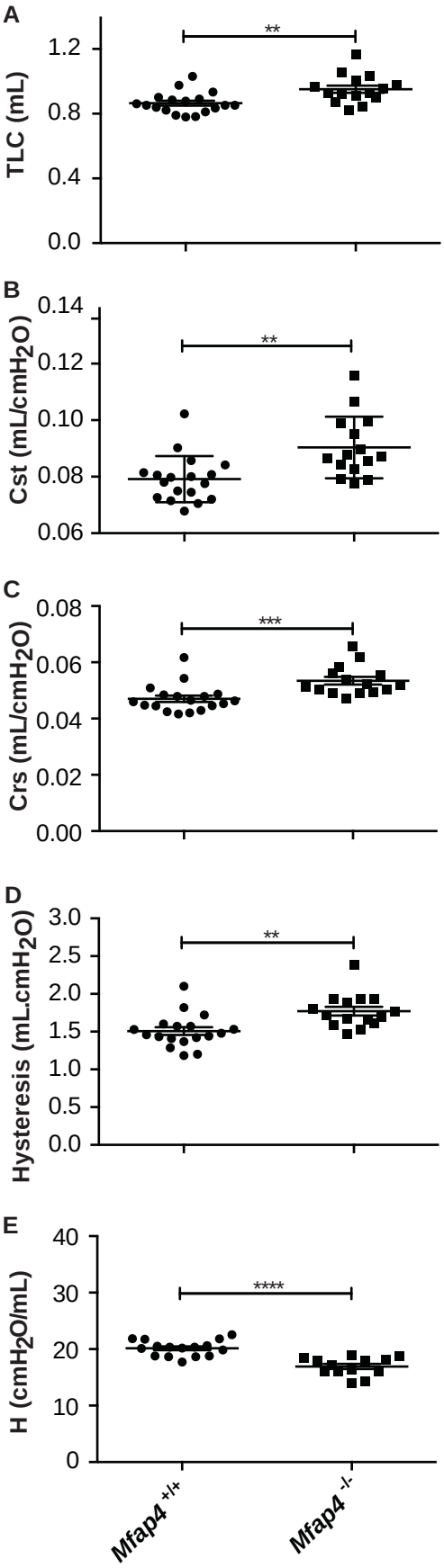
A
TLC (mL)
1.2
0.8
0.4
0.0
**
B
Cst (mL/cmH2O)
0.14
0.12
0.10
0.08
0.06
**
C
Crs (mL/cmH2O)
0.08
0.06
0.04
0.02
0.00
***
D
Hysteresis (mL.cmH2O)
3.0
2.5
2.0
1.5
1.0
0.5
0.0
**
E
H (cmH2O/mL)
40
30
20
10
0
****
Mfap4 +/+
Mfap4 -/-

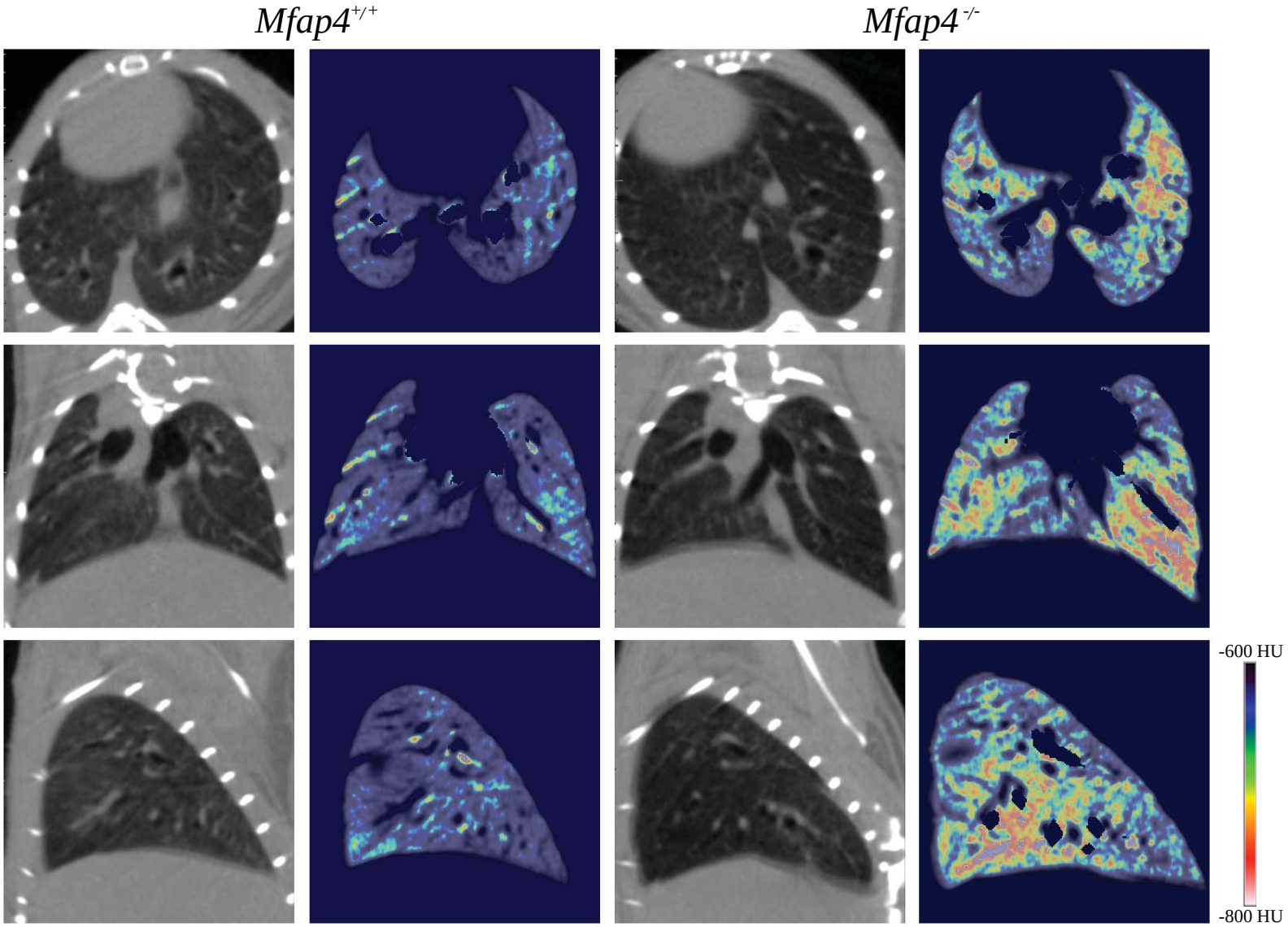
Mfap4$^{+/+}$
Mfap4$^{-/-}$
-600 HU
-800 HU

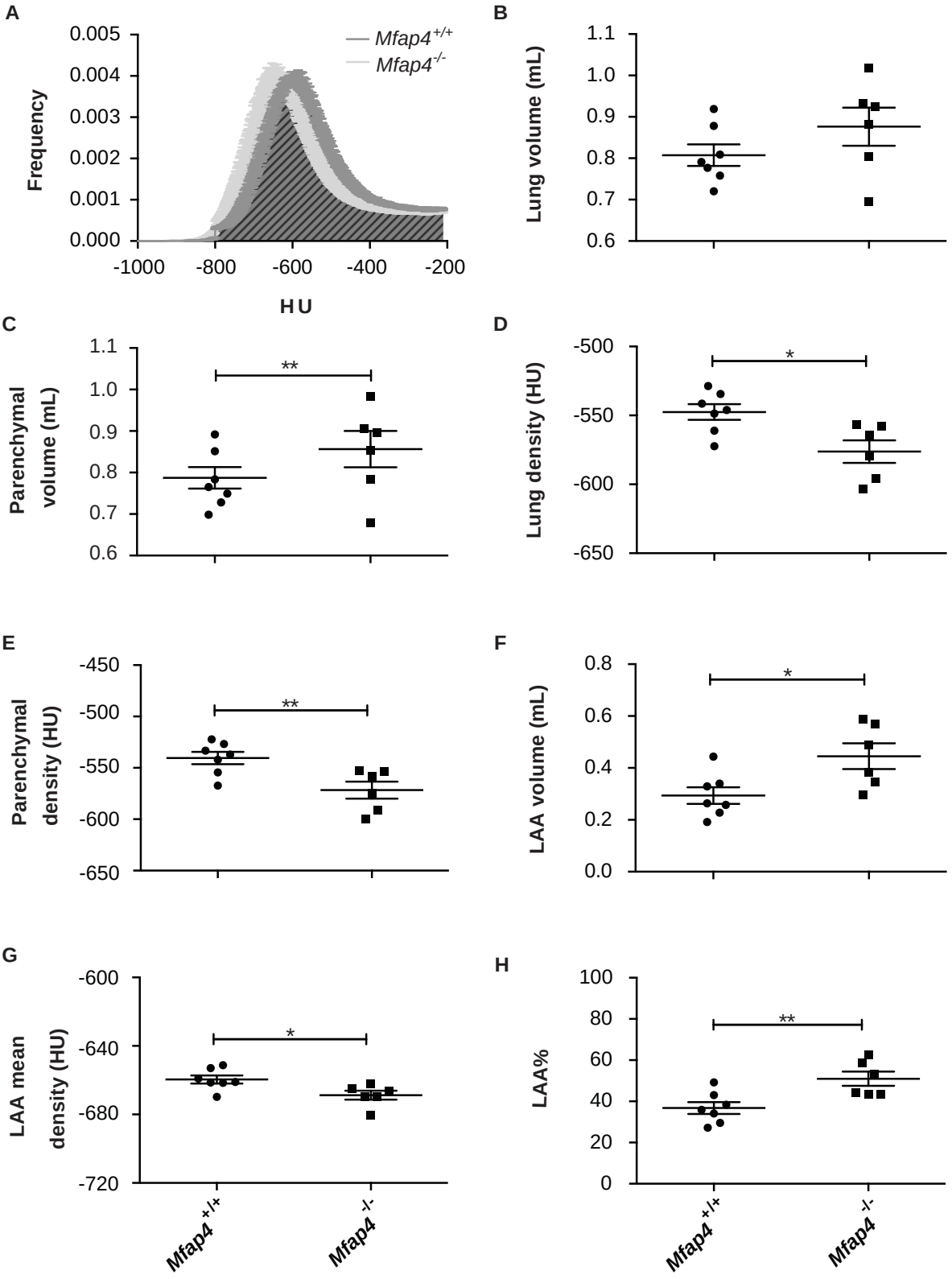
A
Frequency
0.005
0.004
0.003
0.002
0.001
0.000
-1000
-800
-600
-400
-200
HU
Mfap4+/+
Mfap4-/-
B
Lung volume (mL)
1.1
1.0
0.9
0.8
0.7
0.6
C
Parenchymal volume (mL)
**
D
Lung density (HU)
-500
-550
-600
-650
*
E
Parenchymal density (HU)
-450
-500
-550
-600
-650
**
F
LAA volume (mL)
0.8
0.6
0.4
0.2
0.0
*
G
LAA mean density (HU)
-600
-640
-680
-720
*
H
LAA%
100
80
60
40
20
0
**
Mfap4+/+
Mfap4-/-

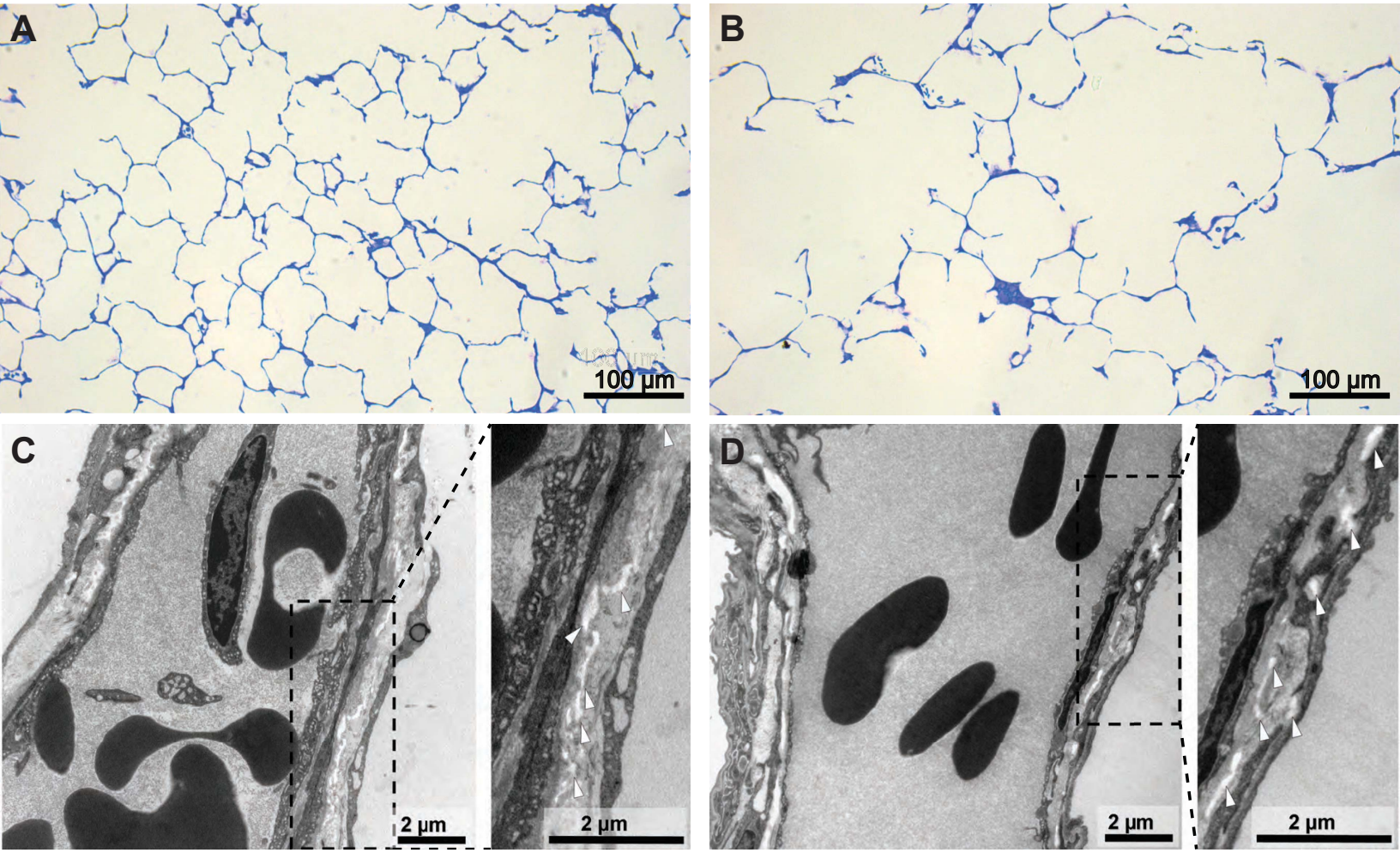
A
100 µm
B
100 µm
C
2 µm
2 µm
D
2 µm
2 µm

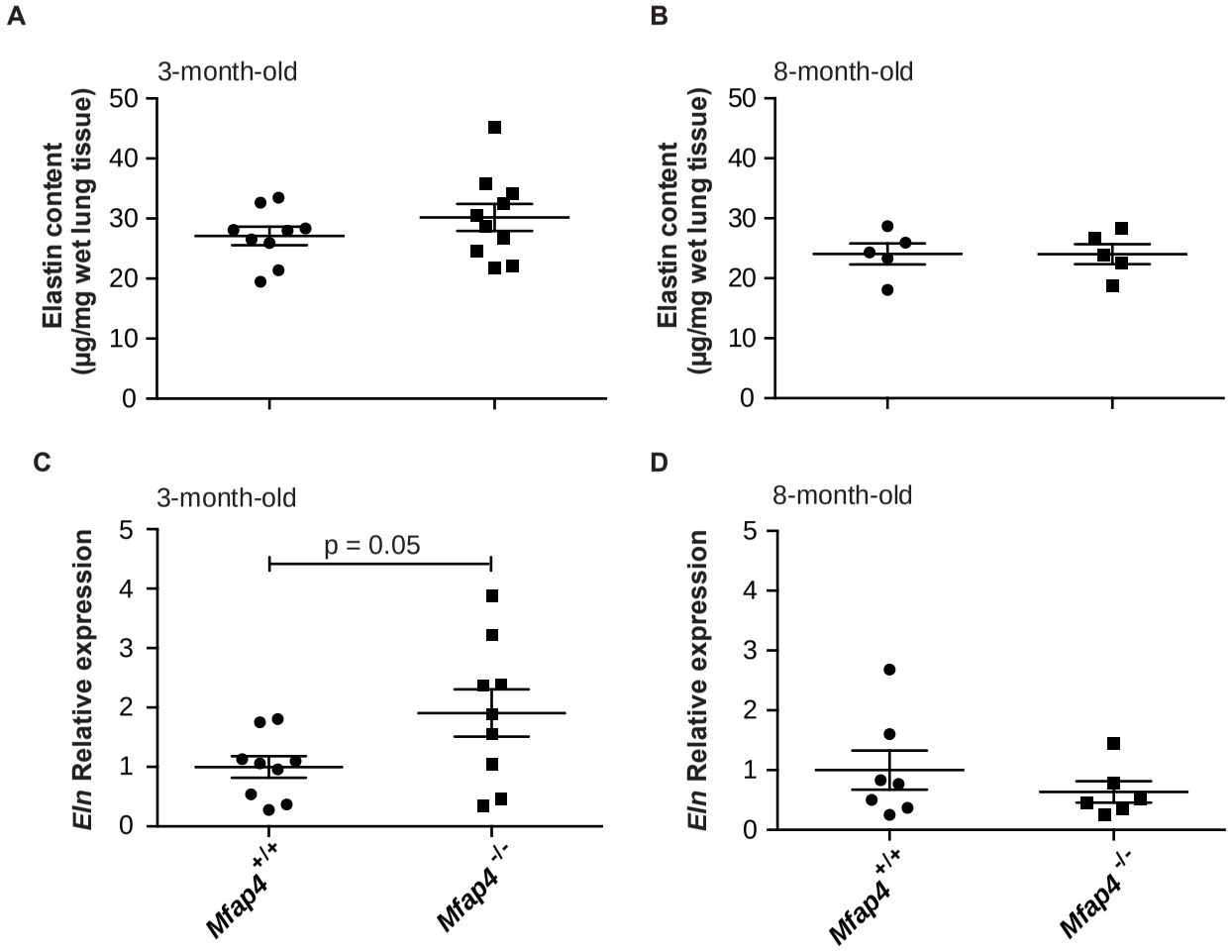
A
3-month-old
Elastin content
(µg/mg wet lung tissue)
50
40
30
20
10
0
B
8-month-old
Elastin content
(µg/mg wet lung tissue)
50
40
30
20
10
0
C
3-month-old
p = 0.05
Eln Relative expression
5
4
3
2
1
0
Mfap4 +/+
Mfap4 -/-
D
8-month-old
Eln Relative expression
5
4
3
2
1
0
Mfap4 +/+
Mfap4 -/-

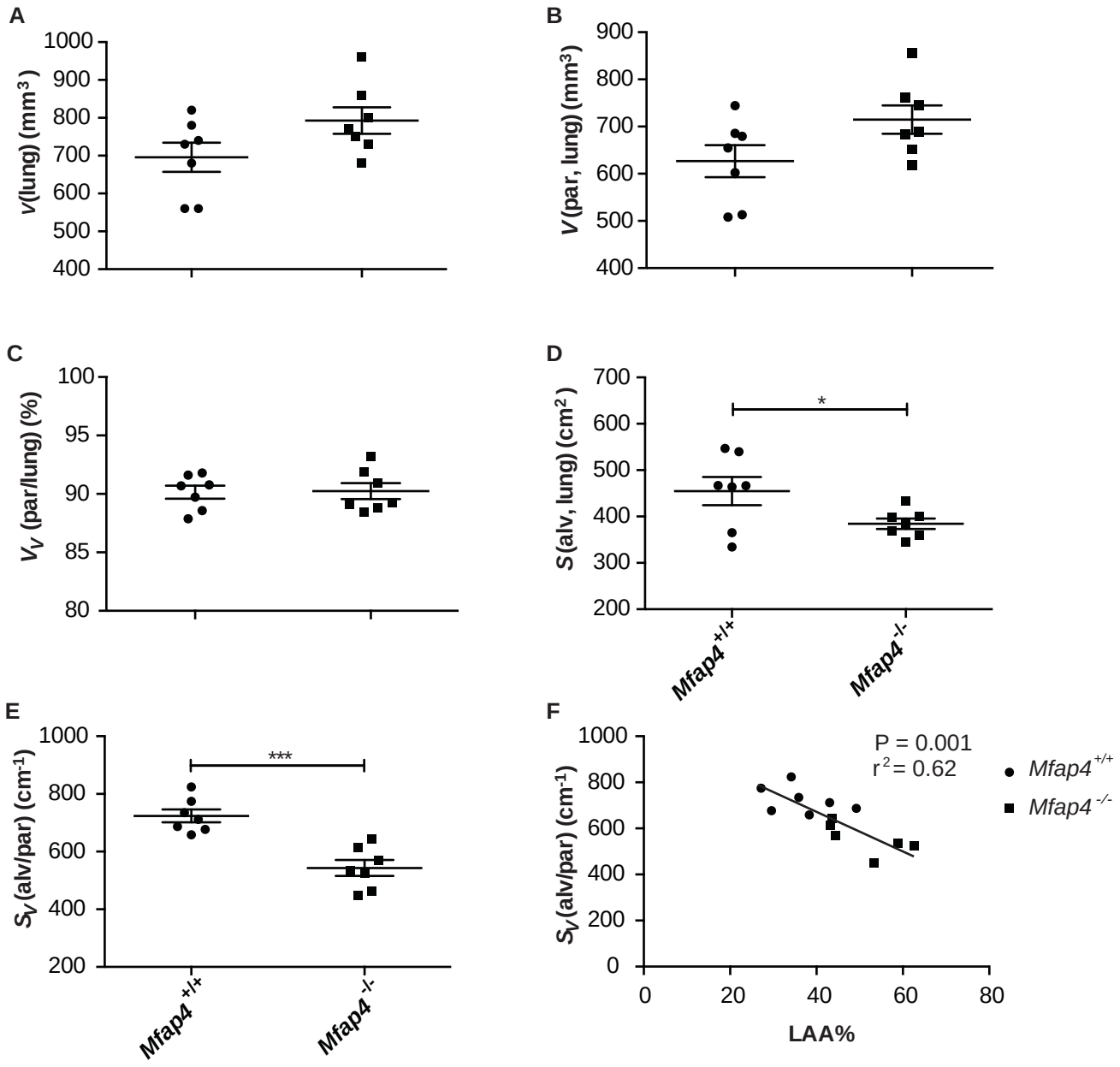
A
V(lung) (mm³)
1000
900
800
700
600
500
400
B
V(par, lung) (mm³)
900
800
700
600
500
400
C
V_V (par/lung) (%)
100
95
90
85
80
D
S(alv, lung) (cm²)
700
600
500
400
300
200
*
Mfap4 +/+
Mfap4 -/-
E
S_V(alv/par) (cm⁻¹)
1000
800
600
400
200
***
Mfap4 +/+
Mfap4 -/-
F
S_V(alv/par) (cm⁻¹)
1000
800
600
400
200
0
P = 0.001
r² = 0.62
Mfap4 +/+
Mfap4 -/-
0
20
40
60
80
LAA%

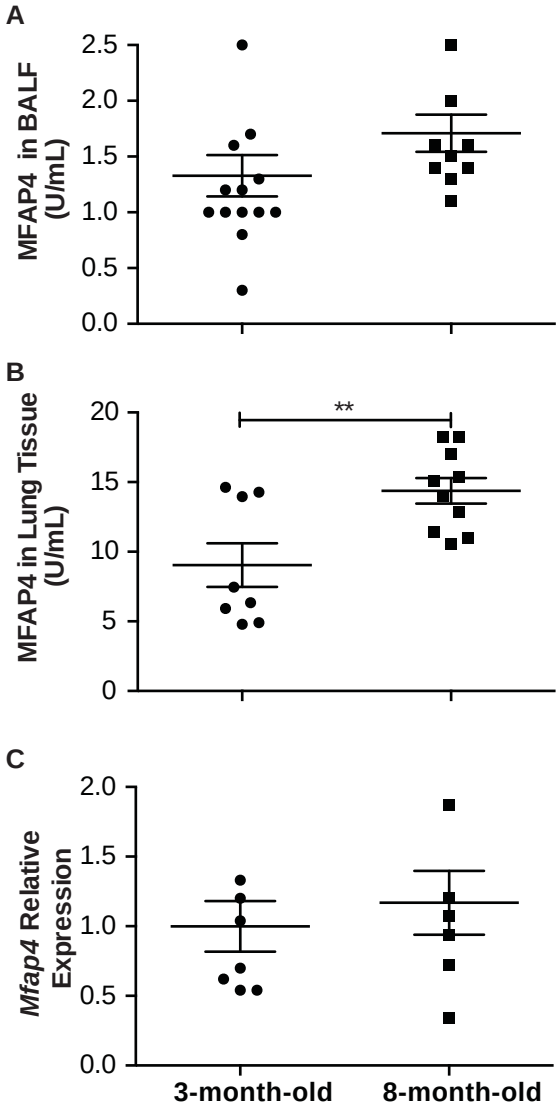
A
MFAP4 in BALF (U/mL)
2.5
2.0
1.5
1.0
0.5
0.0
B
MFAP4 in Lung Tissue (U/mL)
20
15
10
5
0
**
C
Mfap4 Relative Expression
2.0
1.5
1.0
0.5
0.0
3-month-old
8-month-old